

QUSL: Quantum Unsupervised Image Similarity Learning with Enhanced Performance

Lian-Hui Yu^a, Xiao-Yu Li^{†b}, Geng Chen^c, Qin-Sheng Zhu^a, Hui Li^d,
Guo-Wu Yang^{c,e}

^a*School of Physics, University of Electronic Science and Technology of China, Cheng Du, 610054, Si Chuan, China*

^b*School of Information and Software Engineering, University of Electronic Science and Technology of China, Cheng Du, 610054, Si Chuan, China*

^c*School of Computer Science and Engineering, University of Electronic Science and Technology of China, Cheng Du, 610054, Si Chuan, China*

^d*JILA and Department of Physics, University of Colorado, Boulder, 80309-0440, Colorado, USA*

^e*Advanced Cryptography and System Security Key Laboratory of Sichuan Province, Cheng Du, 610103, Si Chuan, China*

Abstract

Leveraging quantum advantages to enhance machine learning capabilities has become a primary focus of research, particularly for complex tasks such as image similarity detection. To fully exploit the potential of quantum computing, it is essential to design quantum circuits tailored to the specific characteristics of the task at hand. In response to this challenge, we propose a novel quantum unsupervised similarity learning method — QUSL. Building upon the foundation of similarity detection triplets and generating positive samples through perturbations of anchor images, QUSL operates independently of classical oracles. By leveraging the performance of triplets and the characteristics of quantum circuits, QUSL systematically explores high-performance quantum circuit architectures customized for dataset features using metaheuristic algorithms, thereby achieving efficient quantum feature extraction with reduced circuit costs. Comprehensive numerical simulations and experiments on quantum computers demonstrate QUSL’s remarkable performance compared to state-of-the-art quantum methods. QUSL achieves reductions exceeding 50% in critical quantum resource utilization while also realizing an enhancement of up to 19.5% in similarity detection correlation across the DISC21, COCO, and landscape datasets. This enables efficient

quantum similarity modeling for large-scale unlabeled image data with reduced quantum resource utilization.

Keywords: Quantum machine learning, Image similarity detection, Metaheuristic algorithms, Unsupervised learning

1. Introduction

Quantum computing represents a paradigm shift in computational capabilities, harnessing the unique properties of quantum mechanics. Currently, quantum computers [1] have entered a stage known as Noisy Intermediate-Scale Quantum (NISQ) computing [2]. Don't use a sledgehammer to crack a nut — quantum resources possess invaluable potential, and quantum computing demonstrates more apparent advantages when dealing with complex tasks [3, 4, 5, 6]. Quantum Machine Learning (QML) [7] has emerged as a noteworthy research focus in the field of image processing, giving rise to representative models such as quantum neural networks (QNN) [8, 9, 10], which have demonstrated remarkable performance in domains like quantum image classification [5, 11]. QML boasts several advantages [8, 12], one of which is its ability to utilize a larger feature space, providing enhanced capabilities for modeling complex patterns in image processing — a crucial aspect for handling high-dimensional tasks such as image processing.

One particularly challenging task in the field of image processing is image similarity detection, which has far-reaching implications for complex applications such as target tracking and object recognition in real-world scenarios [13, 14]. It can be conceptualized as instances of image multiclassification problems characterized by a plethora of unknown classes, each containing only one member. Traditional approaches encounter prominent challenges. With increasing image sizes, the complexity and computational demands of image similarity detection escalate rapidly. This limits the feasibility of employing simple and intuitive algorithms [15, 16] (including Euclidean distance) in large-scale tasks, while the use of data dimensionality reduction techniques inevitably leads to information loss. This indirectly affects the generalization ability of unsupervised and self-supervised learning schemes [17, 18], resulting in unacceptable learning costs for large-scale, high-resolution image datasets.

To tackle these challenges, researchers have begun to explore the potential of quantum computing in image similarity tasks, leading to the development

of the first wave of quantum similarity algorithms [19, 20] and quantum machine learning models [21, 22] specifically tailored to address challenges in image similarity analysis. Pioneering efforts like SliQ [23] have endeavored to establish unsupervised learning processes, where opportunities for enhancing both performance and learning strategies remain. However, a critical challenge in employing quantum computing for image similarity tasks lies in the design and training of high-performance quantum circuits that are tailored to the specific characteristics of the dataset.

The design of quantum circuits presents a specialized optimization challenge [24, 25], aiming to minimize the usage of entanglement gates within the circuit structure’s shallowest possible depth while achieving near-equivalent functionality. Under such task scenarios, obtaining gradient information and ensuring differentiability are challenging, at times entirely unknown for quantum circuits involving intricate quantum state evolution processes. Consequently, addressing this issue through traditional gradient-based optimization methods proves to be notably challenging. Abstracting the optimization problem into a black-box scenario has emerged as an effective strategy to address this challenge [26]. As a result, the introduction of metaheuristic algorithms like evolutionary algorithms [27, 28, 29], which demonstrate self-organization and self-learning characteristics facilitating the design of more advanced quantum circuits [30], has become an efficient approach for quantum circuit design.

In light of the aforementioned challenges and limitations, our research proposes a novel quantum unsupervised similarity learning framework — QUSL, which synergistically integrates the advantages of quantum computing and unsupervised learning. The core motivation behind QUSL is to fully harness the high expressive power of quantum circuits to more effectively process unsupervised image similarity tasks, breaking free from the reliance on classical image similarity algorithms and the performance constraints imposed by parameterized quantum circuit templates.

In QUSL, we introduce an evolutionary algorithm-driven method to explore quantum circuit architectures customized for dataset features. This approach enables the automatic design of quantum circuits that are more efficient than fixed-template parameterized quantum circuits, effectively capturing the intricate patterns within image datasets and enhancing the performance of image similarity detection. Building upon this foundation, we propose a perturbation-based strategy for constructing similarity triplets, allowing QUSL to independently learn and detect image similarities without

relying on classical algorithms, fully leveraging the advantages of quantum computing. QUSL provides a more generalizable and scalable solution for image similarity detection. The contributions of our research can be summarized as follows:

1. QUSL harnesses an evolutionary algorithm-driven method to explore quantum circuit architectures customized for dataset features, achieving more efficient quantum image feature extraction with reduced circuit complexity and learning costs, demonstrating cross-scenario transferability. The code for QUSL is available.
2. Leveraging quantum circuit properties, QUSL incorporates perturbed images to independently construct quantum A, P, N -triplets for unsupervised image similarity detection, offering an adjustable similarity threshold without relying on classical algorithms.
3. Numerical simulations and experiments on quantum computers across DISC21, COCO, and landscape datasets demonstrate QUSL’s superiority over state-of-the-art quantum methods, reducing critical quantum resource utilization by over 50% while enhancing similarity detection correlation up by 19.5%, showcasing its performance advantage in near-realistic scenarios.

2. Background

2.1. Qubits and Quantum Circuits

At the core of quantum computing lies the quantum bit (qubit), which serves as the fundamental unit of information in quantum computation. Unlike classical bits in binary states 0 and 1, A quantum bit $|\psi\rangle$ can simultaneously exist in multiple states due to the principle of superposition, as depicted below

$$|\psi\rangle = \alpha|0\rangle + \beta|1\rangle \quad s.t \ \alpha, \beta \in \mathbb{C} \ \& \ ||\alpha||^2 + ||\beta||^2 = 1. \quad (1)$$

Upon measurement, a probability output is generated, where $||\alpha||^2$ as $|0\rangle$ and with a probability of $||\beta||^2$ as $|1\rangle$. The evolution of quantum bits can be described using unitary transformations acting on single or multiple qubits, where the former allows for arbitrary superposition, and the latter entangles multiple qubits into more complex quantum systems. These unique quantum characteristics grant access to an infinite-dimensional Hilbert space, which is

the fundamental source of the exceptional computational power of quantum computing.

Applying a series of quantum gates to quantum bits yields a quantum circuit, and the design of any quantum computing task involves crafting a specific functional quantum circuit. NISQ quantum computers exhibit heightened sensitivity to larger circuit depths, thus emphasizing lower depths, minimal quantum gate counts, and more efficient utilization of quantum entanglement resources in quantum circuit design [31].

2.2. Quantum Machine Learning and Parametrized Quantum Circuit

QML is a method of performing machine learning tasks using quantum computers. In QML, parametrized quantum circuit (PQC) is a commonly used quantum circuit structure that can adapt to various types of scenes [32].

Similar to selecting appropriate neural network architectures in classical deep learning tasks, choosing the right PQC template is a challenging task. These templates lack any unique handling of datasets or use cases, potentially leading to circuit redundancies and impacts on parallel quantum circuit execution, which are particularly pronounced in multi-qubit tasks. Typically, the parameterized quantum gates are connected with multiple CNOT gates in a ladder-like fashion to form a parameterized layer, and multiple layers of PQCs are cascaded to enhance the expressivity of the overall ansatz.

Another prominent feature of PQC is that the learning process is reflected in the continuous adjustment of parameters, implying that quantum circuits need to be repeatedly executed with the same circuit depth a large number of times[33]. While some effective strategies can mitigate this issue [34], the accumulated total depth remains a key burden in large-scale learning tasks.

2.3. Heuristic Quantum Circuit Design

While templated PQCs offer versatility, they overlook the characteristics of datasets in task scenarios and exhibit redundancy in circuit resources. Designing quantum circuits with higher performance is one of the core tasks in quantum computing.

The formulation of quantum circuit structures embodies an optimization problem, governed by constraints such as the count of quantum physical qubits, adherence to the principles of quantum mechanics for logical consistency, evolution depth, and the composition and quantities of quantum gates. In practical contexts, careful attention must also be paid to the characteristics of the quantum dataset under examination. From this perspective, the

universal variational quantum circuit templates, which disregard the content of the data, essentially undertake only an initial optimization endeavor by simplifying and overlooking numerous constraints.

Evolutionary algorithms have emerged as powerful tools for automatically generating optimal quantum circuits tailored to specific datasets. The study of evolutionary strategies has matured significantly [27, 29, 35] finding widespread applications in diverse fields such as combinatorial optimization [36] and image quantum processing [37].

More specifically, evolutionary algorithms need to select a set of candidate quantum gates and appropriately describe the topology of the quantum circuit to adaptively design circuits. Both of these significantly influence the algorithm’s performance [38]. By strategically evolving, new individuals with higher fitness are obtained until the optimal quantum circuit is found or a predetermined endpoint is reached.

2.4. Unsupervised Quantum Approach for Image Similarity

Silver et al.’s groundbreaking work [23] introduced the first quantum learning approach for effective unsupervised image similarity detection on NISQ quantum computers. This method, rooted in classical unsupervised learning concepts such as Siamese and Triplet networks, utilizes variational quantum circuits for similarity learning and enhances model stability through a projection variance loss function, achieving promising performance on the landscape dataset.

However, the process of constructing triplets in SliQ relies on predefining the Euclidean distance to specify image similarity before training begins. From the perspective of leveraging quantum advantages, the introduction of classical image similarity severely restricts the potential advantages of this quantum model. On the other hand, SliQ employs a parametrized quantum circuit as the model ansatz and adopts a multi-layered hierarchical architecture to enhance its expressive power, yet it still fails to fully exploit the performance advantages of quantum circuits.

3. Quantum Unsupervised Similarity Learning

Motivated by fully exploiting the advantages of quantum computing in unsupervised image similarity tasks, we propose the QUSL framework, which integrates the strengths of quantum computing and unsupervised learning.

Building upon this motivation, QUSL achieves effective generation of quantum A, P, N -triplets without relying on classical algorithms and introduces a heuristic learning process to systematically explore the solution space for realizing high-performance quantum feature mappings.

3.1. A, P, N -Triplet Construction and Quantum Embedding

A, P, N -triplets, a key concept in contrastive learning, have been effectively utilized for image similarity self-supervised learning [39, 40]. Each triplet comprises an anchor image, a positively labeled similar sample, and a negatively labeled dissimilar sample. During the learning process, these triplets are mapped to high-dimensional vectors in the embedding space, capturing the distance between vectors as a representation of similarity. However, unimproved A, P, N -triplets suffer from two drawbacks: inefficient mapping frequency and reliance on the oracle of visual concept discrimination [23]. The oracle, designed to preliminarily assess image similarity based on anchor images, selects positive and negative samples using algorithms or feature combinations. SliQ employs Euclidean distance as the oracle, incurring significant additional classical costs in quantum tasks involving large-scale, high-resolution unlabeled image datasets, thus constraining the quantum advantage.

QUSL use the method of feature interweaving generated by perturbing positive images to improve mapping efficiency and eliminate the use of the oracle of visual concept. Specifically, after anchor image selection is completed, similar images are obtained as positive images by applying slight perturbation to the anchor image as follow

$$\bar{I}[c, i, j] = I[c, i, j] + \mathcal{N}(0, \sigma^2)[c, i, j], \quad (2)$$

where, $I[c, i, j]$ denotes the anchor image with pixel index (i, j) and RGB channel information c , \bar{I} represents positive image, and $\mathcal{N}(0, \sigma^2)$ signifies Gaussian noise with a mean of 0 and variance of σ^2 . Constructing triplets in this stems from a simple fact that is easily overlooked: the most similar image to the anchor image is itself, and perturbation can bring slight differences to the anchor image to produce similarity differences. Gaussian noise, as a widely representative form of noise, exhibits stable interference effects on image features [41], making it a universal source of perturbation. In addition, QUSL adopts the strategy of utilizing feature interweaving to reduce the mapping process.

To adapt the quantum model to the task of RGB image similarity, classical images need to be quantum-embedded. Considering the limitations of the number of quantum bits in the NISQ era and the processing characteristics of quantum circuit models for image features, quantum amplitude embedding [42] is introduced to encode input features into physical quantum bits as follows

$$|\psi\rangle = \sum_{i=1}^{\lceil \log_2 6N^2 \rceil} p_{i-1} |i-1\rangle, \quad (3)$$

where, $|\psi\rangle$ represents the quantum state obtained by amplitude embedding a pair of training set. For an image of size $N * N$, p_i represents the i -th element of the training set vector, which is a normalized vector of length $6N^2$ after feature interweaving of the triplet. Thus, amplitude embedding saves a large number of quantum bits and preserves the complete image features mapped to the Hilbert space without the need for compression methods such as PCA. From the perspective of quantum information, feature interweaving of images in the triplet also results in complex entanglement between different image features, thereby augmenting the representation of image features [43]. The above process is shown in the Fig.1.

In summary, QUSL achieves efficient formal processing and quantumization of classical image features.

3.2. Dataset-Oriented Quantum Learning Circuit Construction

Heuristic quantum circuit design methodologies, such as evolutionary algorithms, can holistically address multiple constraints to determine the nearly optimal quantum state evolution process. The formulation of fitness functions for these algorithms should consider the attributes of enhanced A, P, N -triplets.

Unlike conventional triplets [39], the quantum version's mapping procedure cannot be simply represented as the projection of three vectors onto a two-dimensional plane. This complexity stems from the incorporation of training sets, which introduces entanglement among image features, disturbing the direct correspondence between the mapped vectors and the features.

To reconcile this disparity, a corrective term must be included in the loss function for classical mapping to ensure projection coherence [23]. Based on the conceptualized quantum circuit model, the training sets of A, P, N -triplets are embedded into the Hilbert space and encapsulated by the probability distributions obtained from measuring the first four qubits of the

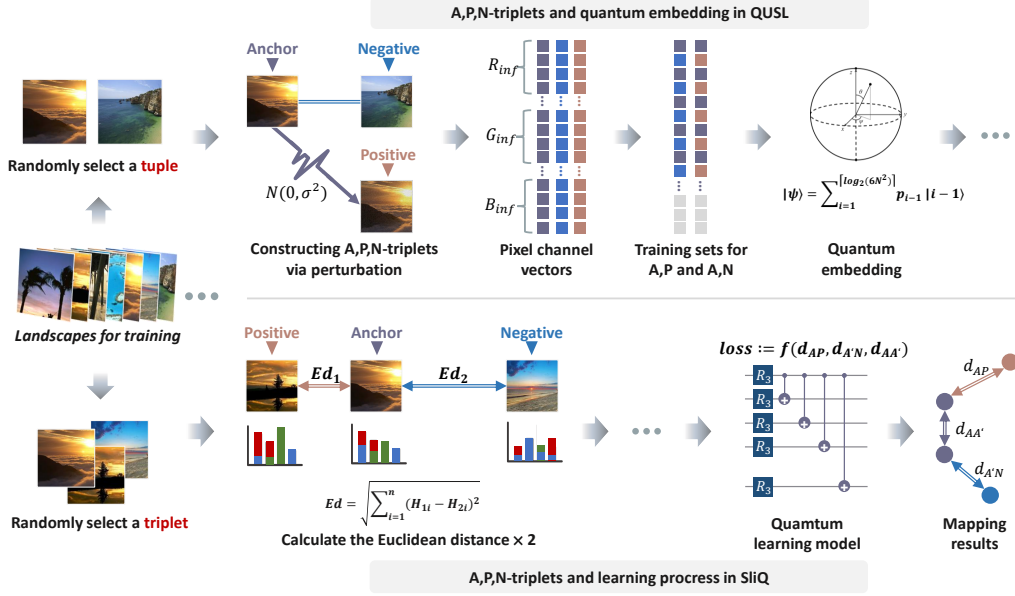


Figure 1: The preprocessing of A, P, N -triplets involves quantum embedding in QUSL. For comparison, the triplet construction and learning process of SliQ are illustrated below the figure. The specific meanings of the equations in the figure can be found in Eq.2, Eq.3, and Eq.7.

quantum circuit across two mappings. By combining the practical significance of fitness and the rectified mapping relationship, the fitness function, designed to maintain projection consistency, is formulated as follows

$$F_{obj} := \frac{1}{\alpha(l_{QM}) + \beta\Delta}, \quad (4)$$

where, α and β represent harmonic hyperparameters employed to determine the equilibrium of the correction term. The quantum mapping is intended to yield analogous outcomes to the classical mapping process. Therefore, l_{QM} is defined as the discrepancy in vector distance as specified in the classical A, P, N -triplets method, formulated as

$$l_{QM} = (|A_{px} - P_x| + |A_{py} - P_y|) - (|N_x - A_{nx}| + |N_y - A_{ny}|), \quad (5)$$

where, A_{px} , A_{py} , P_x , P_y denote the measure expectation of the first to fourth qubits of the training sets comprised of anchor images and positive images subsequent to their traversal through the quantum circuit. Similarly, N_x , N_y ,

A_{nx} , A_{ny} signify the measure expectation of the first to fourth qubits of the training sets formed by anchor images and negative images after undergoing the quantum circuit.

The correction term Δ is defined as the discrepancy in distance between the vectors derived from the two mappings of anchor images within the two training sets, expressed as follows

$$\Delta = |A_{px} - A_{nx}| + |A_{py} - A_{ny}|. \quad (6)$$

The fitness function takes into account the attributes of evolutionary algorithms and mitigates the adverse impacts resulting from the enhanced efficiency of A , P , N -triplets.

Designing evolutionary algorithms for quantum circuits poses challenges due to the unique characteristics of quantum circuits, such as performance symmetry and constraints in heterogeneous quantum circuits.

Performance symmetry arises from the principle of qubit permutation symmetry, where the numbering and arrangement of qubits do not affect the system's evolution operator, maintaining system equivalence. This can lead to heterogeneous quantum circuits achieving similar or identical performance, hindering population diversity in evolutionary algorithms [44]. To mitigate this issue and maintain comprehensive coverage of the quantum circuit structure solution space, tournament selection can be employed, effectively reducing the survival rate of similar redundant individuals and balancing population diversity and convergence.

Performance constraints, another fundamental issue in quantum circuit design, require a holistic consideration of various aspects of quantum circuit performance evaluation. Non-dominated sorting [45] categorizes the population based on their support, with individuals within the same category being non-dominated. This approach generates diverse trade-off solutions, focusing on the Pareto front. When applied to quantum circuit design, non-dominated sorting simplifies population complexity and prevents the generation of high-depth, complex entangled quantum circuits. The synergistic application of tournament selection and non-dominated sorting ensures expansive exploration and expedites convergence to local depth. The comprehensive evolutionary strategy is illustrated in Fig. 2.

In conclusion, QUSL utilizes a comprehensive evolutionary strategy to explore high-performance quantum circuits that conform to the constraints of image similarity tasks while ensuring projection consistency in fitness settings.

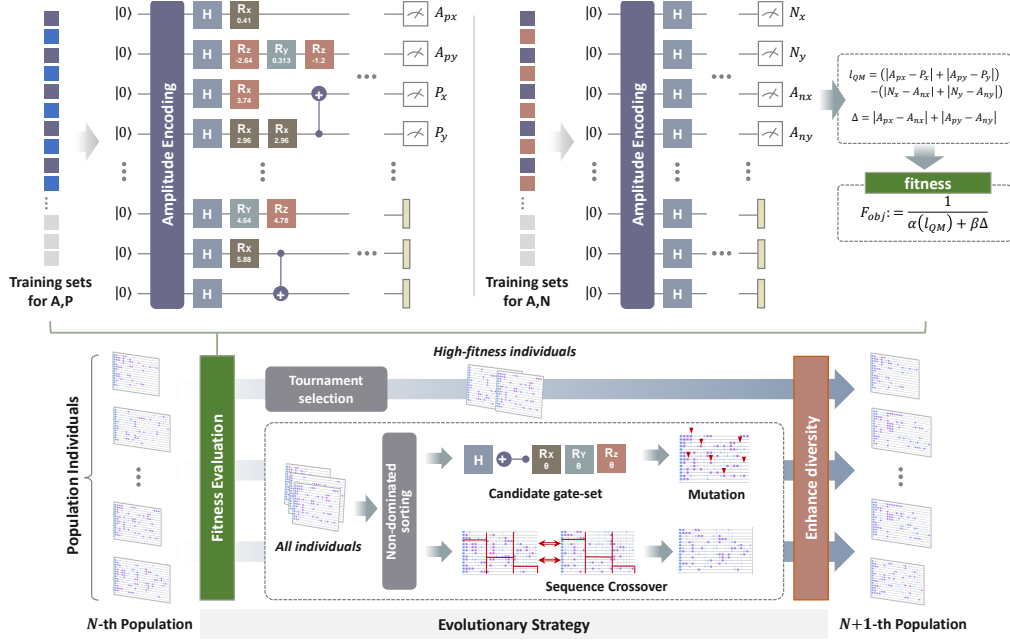


Figure 2: The evolutionary strategy for quantum circuits design in QUSL. To compactly illustrate the strategy, the figure does not depict the details of the components in the evolutionary algorithm.

3.3. Image Similarity Performance Evaluation for Quantum Model

In the domain of unsupervised image similarity assessment and similar tasks, correlation analysis is frequently employed as a primary evaluation metric [46]. Correlation analysis evaluates model performance by assessing the consistency between the similarity scores generated by the model and the actual similarity between images, thereby addressing the limitations associated with directly comparing score disparities among different models. This classic comparative approach exhibits high versatility and can be directly transferred to the quantum domain.

In QUSL, model performance is evaluated by computing the Spearman correlation coefficient between the similarity assessment scores outputted by the quantum model and the Euclidean distance as follow

$$Ed = \sum_{i=1}^N \sqrt{(R_{(2i)} - R_{(1i)})^2 - (G_{(2i)} - G_{(1i)})^2 - (B_{(2i)} - B_{(1i)})^2}, \quad (7)$$

where $(R_{(2i)}, G_{(2i)}, B_{(2i)})$ and $(R_{(1i)}, G_{(1i)}, B_{(1i)})$ represent the RGB values of

the i -th pixel in the reference image and the image to be compared, respectively. In practical computations, this process is often simplified by utilizing methods such as color frequency histograms to condense pixel information for rapid calculations. In this case, the Euclidean distance can be expressed as $E_d = \sqrt{\sum_{i=1}^n (H_{1i} - H_{2i})^2}$. Here, H_{1i} and H_{2i} represent the channel information in the i -th interval of the two histograms, with n denoting the total number of intervals in each histogram.

The computation of similarity assessment scores follows the following approach: The improved A, P, N -triplets method, which employs feature entanglement, is simplified to consider only the scenario involving anchor images and comparison images for similarity assessment. By exchanging the tuple labels of the anchor image and the positive image, this approach enables the quantification of the similarity between two images. Therefore, the similarity assessment scores S_{sim} are defined as the difference between the vectors obtained from two mappings of the anchor image and the positive image after feature interweaving as follow

$$S_{sim} := \mathcal{F}(A^{(1)}, A^{(2)}, P^{(1)}, P^{(2)}), \quad (8)$$

where $A^{(i)}$ and $P^{(i)}$ represent the vectors obtained from the anchor image and positive image, respectively, in the i -th mapping. \mathcal{F} denotes the operator acting on the four sets of vector coordinates obtained during the two mapping processes, representing the differences in coordinates between the two mappings. For simplicity, cumulative coordinate differences can be used for computation. When the coordinates from the two mappings are identical, S_{sim} takes the minimum value of 0, indicating complete similarity between the anchor image and the positive image. Conversely, when significant coordinate changes occur, S_{sim} takes large positive values, with the numerical magnitude positively correlated with the degree of difference between the anchor image and the positive image. The range of S_{sim} and its correlation with image similarity are analogous to the Euclidean distance Ed , thus making it suitable for Spearman correlation computation. Let $\mathbf{S} * rg$ denote the sorted collection of $S * sim$ series outputted by the quantum model for a sequence of n pairs of similarity detection images, and let \mathbf{ED}_{rg} denote the sorted collection of Euclidean distances Ed obtained for the corresponding image pairs sequence. Then, the Spearman correlation coefficient ρ is defined as

$$\rho = \frac{cov(\mathbf{S}_{rg}, \mathbf{ED}_{rg})}{\sigma(\mathbf{S}_{rg})\sigma(\mathbf{ED}_{rg})} = \frac{\sum_{i=1}^n (S_{sim(i)} - \overline{\mathbf{S}_{rg}})(Ed_{(i)} - \overline{\mathbf{ED}_{rg}})}{\sqrt{\sum_{i=1}^n (S_{sim(i)} - \overline{\mathbf{S}_{rg}})^2} \sqrt{\sum_{i=1}^n (Ed_{(i)} - \overline{\mathbf{ED}_{rg}})^2}}, \quad (9)$$

where, $S_{sim(i)}$ and $Ed_{(i)}$ denote the i -th elements of \mathbf{S}_{rg} and \mathbf{ED}_{rg} , respectively, while $\overline{\mathbf{S}_{rg}}$ and $\overline{\mathbf{ED}_{rg}}$ represent the mean values of elements in the two sets. The Spearman correlation coefficient, by definition, ranges from -1 to 1 , with 0 indicating no correlation, 1 denoting perfect positive correlation, and -1 representing perfect negative correlation. Models exhibiting higher positive correlation values demonstrate relatively better performance. In subsequent experiments and comparative analyses, this coefficient will be utilized to assess the performance of the quantum image similarity model.

4. Experiments and Result

This section presents a rigorous experimental evaluation of the QUSL model across diverse datasets, providing comprehensive empirical evidence to demonstrate its effectiveness, robustness, and superiority compared to state-of-the-art quantum methods.

4.1. Experiment Framework

In the domain of unsupervised image similarity tasks, the Flickr landscape, COCO, and DISC21 datasets have been selected for training and testing purposes. Flickr landscape [47], comprising unlabeled colorful images depicting diverse natural landscapes, serves to explore the performance of QUSL in image similarity detection and feature learning without explicit category labels. COCO [48], widely used for tasks like object detection and segmentation, offers a large-scale collection of labeled images with varied scenes and objects. By removing labels from COCO, we aim to scrutinize QUSL’s unsupervised learning capability further while assessing its adaptability to diverse and complex image datasets. DISC21 [49], explicitly designed for image similarity detection and utilized as a benchmark in the NeurIPS’21 Image Similarity Challenge (ISC2021), emphasizes image transformations, including automated conversion, manual editing, and ML-based operations. This dataset is instrumental in evaluating QUSL’s real-world applicability, particularly in social media contexts. The essential details of these datasets and the experimental configurations in our task are outlined in Table 1.

The experimental setup was configured using Python3, incorporating a hybrid combination of the Qiskit and MindSpore [50] frameworks. Numerical simulations were executed on a workstation (CPU: Intel I9 9900k, GPU: GTX3090). Guided by pre-experiment instructions, an evolutionary algorithm tailored for quantum circuits was deployed, featuring a population size

Table 1: Datasets with basic setup used.

Dataset	Categories Used	Patch Size	Qubit Used
landscape	7 object categories ^a	$80 \times 80 \times 3$	14
COCO	80 object categories ^{ss}	$\leq 800 \times 800 \times 3^b$	14
DISC21	21 object categories	$\leq 800 \times 800 \times 3$	14

^a landscape, COCO, and DISC21, do not utilize existing labels in the experiments.

^b COCO and DISC21 feature a plethora of image dimensions; herein present the maximum dimensions.

of 20 and a maximum evolution generation of 20. The gate set constituting the quantum circuit comprised $R_X, R_Y, R_Z, H, CNOT$. Images within the training set underwent uniform processing to ensure consistent dimensions. The number of qubits utilized for each scenario is also delineated in Table 1. Following the selection of anchor images, random images from the training set were chosen to form A, P, N -triplets. During training, any potential labels in the dataset were disregarded to align with the unsupervised setting. For all models trained on similarity tasks, 1000 similarity tests were conducted, and model performance was assessed using correlation detection.

4.2. Evaluation and Analysis

To determine the optimal perturbation level for the QUSL algorithm, we conducted a series of preliminary experiments on the landscape dataset, evaluating the algorithm’s performance across different perturbation levels, characterized by the parameter σ .

Five independent experimental runs were carried out at each perturbation level, with the results presented in Fig.3 and Table.2.

Table 2: Performance of the QUSL under varying levels of perturbation.

Level	Correlation performance ^a					Mean value
0	0.830 ^b	0.762	0.821	0.803	0.806	0.804(± 0.024) ^c
5	0.837	0.829	0.889	0.814	0.822	0.838 (± 0.026)
10	0.823	0.828	0.820	0.819	0.823	0.823(± 0.024)
15	0.817	0.791	0.803	0.853	0.857	0.824(± 0.025)

^a Five independent training and testing sessions were conducted at each perturbation level, with correlation values reported to three decimal places.

^b The bold numbers indicate the highest correlation achieved in each experimental group.

^c “ \pm ” represents the standard deviation, reflecting the dispersion of sample data, as it does elsewhere in this paper. A smaller value indicates higher stability of model performance.

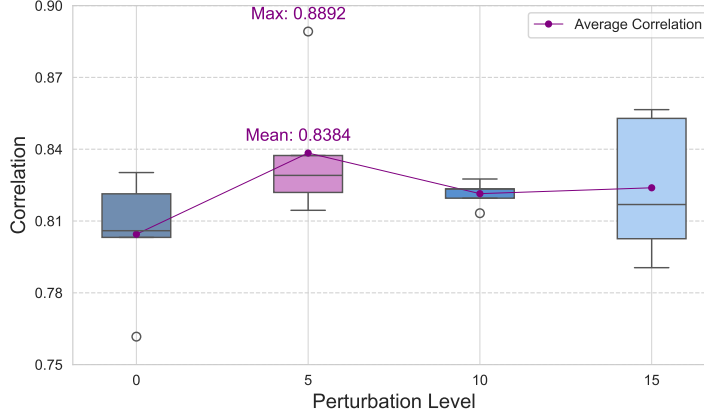


Figure 3: Performance of the QUSL on the landscape dataset under varying levels of perturbation.

In comparative experiments conducted under identical experimental conditions, when the perturbation level was set to 5 (indicated by purple shading in the Fig. 3), the QUSL model achieved the best training performance of 0.8892, exhibiting the highest average training effectiveness and acceptable data dispersion. In contrast, the performance under other conditions showed lower training results and instability. Furthermore, the perturbation level has a significant impact on model performance, resulting in a performance discrepancy of up to 12% in terms of correlation.

Therefore, by comprehensively considering relevant performance metrics, including maximum performance, average performance, and robustness, a perturbation level of 5 can be selected as the parameter setting for subsequent experiments. Moreover, the perturbation level can serve as a controllable threshold for image similarity during the learning process, or an adaptive approach can be employed to more precisely regulate the perturbation level.

Controlled experiment were designed to comprehensively examine the performance efficacy and robustness of QUSL on three datasets (landscape, COCO, and DISC21), while concurrently benchmarking against SliQ. QUSL and SliQ underwent five training sessions and correlation tests of equal scale on each of the three datasets, recording the best results obtained during the training process, which are presented in Fig. 4 and Table. 3.

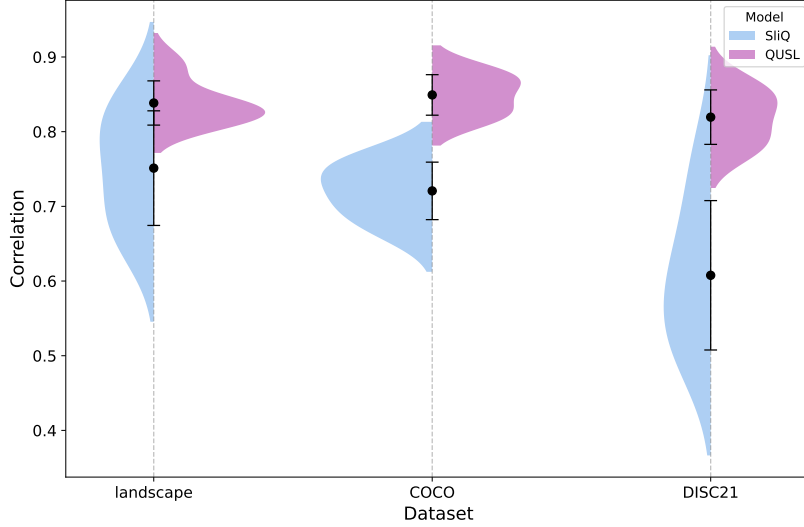


Figure 4: Performance evaluation of QUSL and SliQ across different datasets. In the violin plot, the blue and purple areas represent the distribution states of correlation obtained by SliQ and QUSL, respectively.

Table 3: Performance comparison between SliQ and QUSL based on five independent experiments.

Dataset	landscape		COCO		DISC21	
Correlation ^a	SliQ	QUSL(ours)	SliQ	QUSL(ours)	SliQ	QUSL(ours)
1st	0.835	0.889	0.757	0.876	0.758	0.861
2st	0.814	0.837	0.757	0.875	0.649	0.847
3st	0.758	0.829	0.722	0.852	0.593	0.825
4st	0.692	0.822	0.699	0.822	0.592	0.787
5st	0.657	0.814	0.668	0.821	0.528	0.777
Mean value	0.751 (± 0.078)	0.838 (± 0.031)	0.721 (± 0.035)	0.849 (± 0.027)	0.624 (± 0.096)	0.819 (± 0.037)
Optimization rate	-	$\uparrow 8.7\%$	-	$\uparrow 12.8\%$	-	$\uparrow 19.5\%$

^a The correlation obtained from multiple experiments is sorted in descending order.

In all three datasets, QUSL demonstrated significant enhancements in both performance and stability. In comparison to SliQ, QUSL exhibited a remarkable improvement in correlation, with increases ranging from a minimum of 8.7% to a maximum of 19.5%. Regarding stability, QUSL displayed a distinct advantage over SliQ in terms of the standard deviation of performance means, particularly evident in the DISC21 dataset, where SliQ’s performance exhibited substantial fluctuations, while QUSL’s stability re-

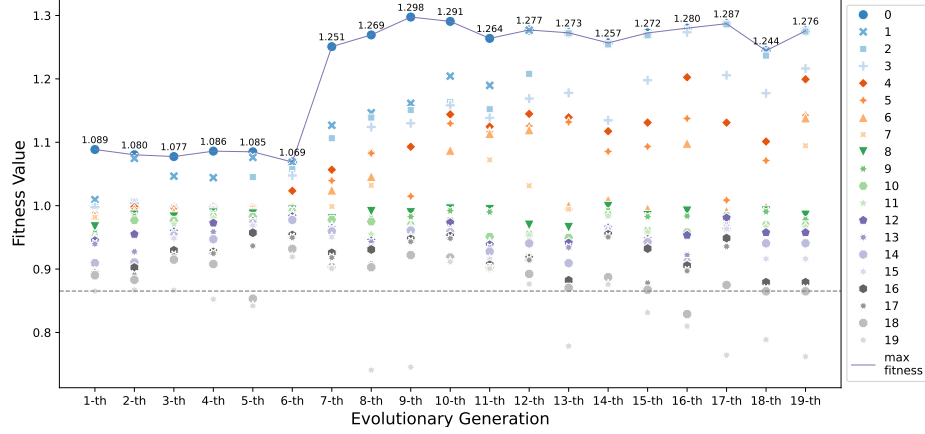


Figure 5: Fitness trajectory of individuals across generations during the evolutionary process in landscape. The figure annotates the fittest individuals in each generation of 20 individuals with corresponding values. The dashed line below the image represents the lowest fitness among individuals in the first generation. Given the tendency of evolutionary algorithms to converge towards optimization, individuals below the dashed line are eliminated during the evolution process.

maintained largely unaffected by the application scenarios.

QUSL’s superior performance and stability can be primarily attributed to its capacity to adapt to dataset characteristics through the evolutionary process. Conversely, the parameter adjustment of template-based variational quantum circuits may encounter difficulties in capturing the intrinsic properties of the dataset, resulting in performance degradation under equivalent training conditions. This set of experiments serves to highlight the transferability of QUSL across various domains.

A series of experiments were designed to further investigate the detailed training process of QUSL, showcasing its accuracy and interpretability.

Fig.5 illustrates the fluctuation of fitness values for all individuals within one evolutionary cycle. It is important to note that to ensure broad adaptability of individuals to all image combinations within the dataset, QUSL employs random sampling of the dataset during the training process, assembling multiple sets for fitness evaluation. This approach leads to the stabilization of the best individual’s fitness within a certain range, rather than strictly increasing monotonically and ultimately converging during the evolution process. It is evident that as the number of generations increases, the fitness of the best individual improves, demonstrating the success of the evolutionary process.

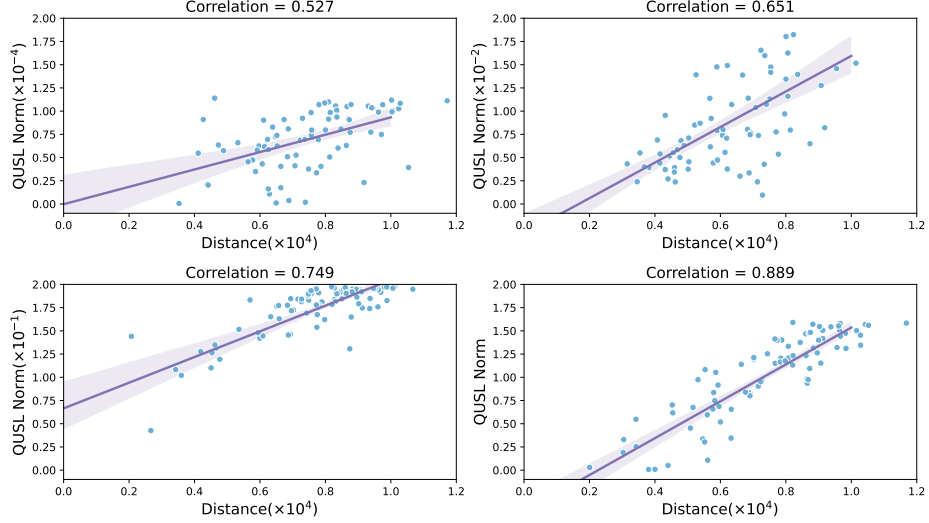


Figure 6: Relationship between euclidean distance and QUSL norm, the output of method, across different correlation levels. The purple line represents the regression analysis and corresponding confidence interval of the scatter plot, directly reflecting the correlation between the similarity of QUSL and the Euclidean distance.

It is worth noting that during the evolution process, there are still individuals with significantly different quantum circuit structures but no apparent difference in fitness performance. A typical example of this scenario is demonstrated in Appendix B. This further demonstrates the threat of low population diversity in metaheuristic quantum circuit design due to the inherent characteristics of quantum circuits.

The validity of using correlation as a model performance metric can be verified by the correspondence between the distribution of image similarities and their correlation. The results of this set of experiments are presented in Fig.6, with the validation conducted on the landscape dataset.

As the number of generations increases, the correlation between QUSL norm and Euclidean distance also gradually improves, reaching a maximum correlation of 0.889 in this evolution, which is a significant advantage compared to SliQ. To more clearly demonstrate the correctness of the correlation metric, Fig.7 and Fig.8 respectively illustrate the true distribution of images in the models with the best correlation on the COCO and DISC21 datasets.

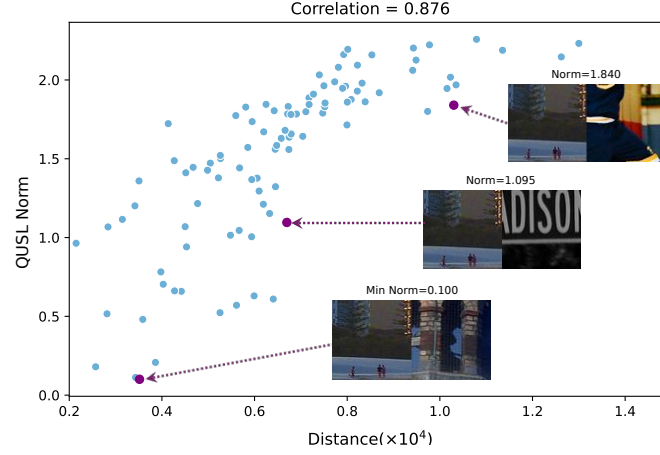


Figure 7: Results of QUSL on the COCO. The model’s correlation is 0.876, achieved by the optimal individual during the evolution process. When QUSL norm reaches its minimum value of 0.1, QUSL identifies the most similar images in the current test set.

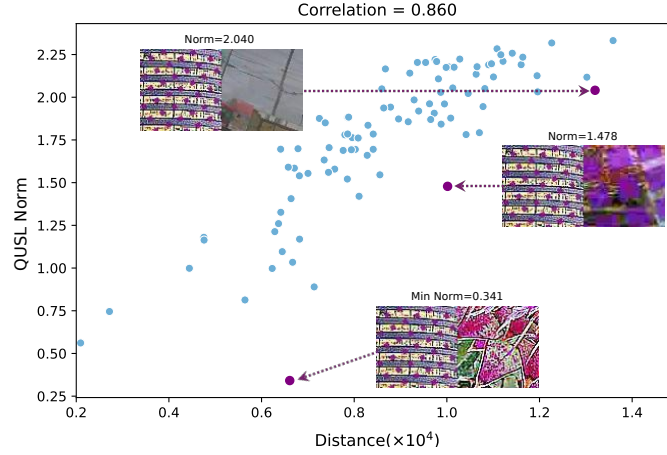


Figure 8: Results of QUSL on the DISC21. The model’s correlation is 0.860. When QUSL norm reaches its minimum value of 0.341, QUSL identifies the most similar images in the current test set.

As illustrated in the figures, the Euclidean distance and QUSL norm exhibit a positive correlation, and images with smaller QUSL norm values demonstrate more significant visual similarity. This reflects the alignment between the image similarity determined by Euclidean distance and the image similarity assessed by QUSL.

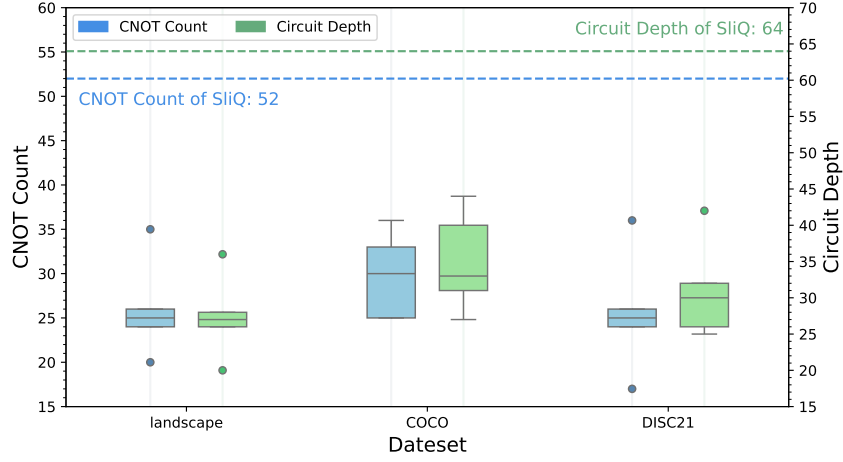


Figure 9: CNOT count and circuit depth utilized in the quantum circuit of QUSL. The green and blue dashed lines above the plots represent the circuit depth and CNOT count, respectively, of the variational quantum circuit templates used by SliQ, which remain unchanged across different datasets.

It is crucial to highlight that the test set is randomly sampled from the dataset, and consequently, there may be an absence of image combinations that are visually indistinguishable to human perception. Nevertheless, the fluctuations in the similarity values generated by QUSL can still offer valuable insights into the variations in visual similarity among the images. The aforementioned experiments collectively validate the appropriateness of employing correlation as a model performance evaluation metric and further corroborate the model’s correctness.

In terms of core quantum resources, a set of numerical experiments and experiments on quantum computers were designed to evaluate the comparison between QUSL and SliQ in terms of quantum circuit depth and CNOT count. Fig.9 and Table.4 illustrates a comparison of the quantum circuit performance between the two approaches.

Across the landscape, COCO, and DISC21 datasets, the quantum circuits derived through QUSL exhibit reductions of around 50% in both CNOT counts and circuit depth. This indicates that within acceptable fluctuations, the quantum circuits generated by QUSL significantly outperform SliQ in key performance indicators, directly contributing to the model’s advantage in quantum resource utilization. The demonstration of high-performance quantum circuits is presented in Appendix A.

Table 4: CNOT count and circuit depth utilized in the quantum circuit of QUSL.

Dataset	Critical quantum resource performance					
	landscape		COCO		DISC21	
	Correlation	CNOT count	Circuit depth	CNOT count	Circuit depth	CNOT count
1	35	36	30	33	17	26
2	20^a	20	33	40	24	30
3	26	28	36	44	25	25
4	24	27	25	27	36	42
5	25	26	25	31	26	32
Mean value	26.0 ^b (±4.9)	27.4(±5.1)	29.8(±4.2)	35.0(±6.2)	25.6(±6.3)	31.0(±6.1)
Optimization rate	↓ 50.0% ^c	↓ 57.2%	↓ 42.7%	↓ 45.3%	↓ 50.8%	↓ 51.6%

^a Bold text indicates the best-performing parameters within a set of experiments.

^b The CNOT count and circuit depth are both integers, mean value merely reflects the relative performance of the corresponding quantum circuits.

^c The optimization rate refers to the decrease ratio of the average CNOT count and circuit depth compared to their respective values in SliQ, where the CNOT count is 52 and the circuit depth is 64.

A set of validation experiments on quantum computers demonstrated the practical usability and significant advantages of QUSL in the NISQ era. Table 5 presents a comparison of the running times between the high-performance quantum circuits used in QUSL and the template circuits employed in SliQ.

Through five independent circuit runs on the three datasets, it can be observed that QUSL consistently reduces the running time of individual quantum circuits. The time advantage at the single-circuit level is significantly amplified by the large number of circuit runs during the training process, which is reflected in the model’s training efficiency and practical application efficiency. This advantage of QUSL becomes more evident in large-scale image similarity tasks.

Through numerical simulations and a series of experiments on quantum computers, the QUSL algorithm demonstrates robust high performance in image similarity tasks, achieving higher average correlations across multiple datasets and significantly improving stability on challenging datasets like DISC21. Detailed analysis of the training process reflects QUSL’s effective ability to capture visual similarities among images. Combined with validation on quantum computers, QUSL significantly reduces quantum circuit depth and CNOT counts compared to SliQ’s variational template. The aforementioned advantages directly translate into improved utilization of quantum

Table 5: Comparison of the running times of optimal quantum circuits on real quantum computers.

Dataset	landscape		COCO		DISC21	
Run time(s) ^a	SliQ	QUSL	SliQ	QUSL	SliQ	QUSL
1	1.64	1.55	1.60	1.50	1.67	1.48
2	1.73	1.59	1.73	1.61	1.70	1.49
3	1.76	1.60	1.76	1.72	1.70	1.51
4	1.21	1.64	1.76	1.72	1.74	1.65
5	1.90	1.80	1.80	1.73	1.74	1.75
Mean value	1.77 ^c (± 0.089)	1.64 (± 0.087)	1.77 (± 0.080)	1.66 (± 0.089)	1.71 (± 0.027)	1.58 (± 0.109)
Optimization rate	-	\downarrow 0.13	-	\downarrow 0.11	-	\downarrow 0.13

^a Five independent running times sorted in ascending order.

resources in NISQ environments and achieve higher performance and efficiency in large-scale image similarity scenarios that are closer to real-world applications.

Overall, QUSL emerges as a high-performance method for image similarity detection, surpassing current state-of-the-art quantum image similarity detection methods in terms of stability, correlation, and quantum resource efficiency.

5. Discussion and Futher Work

Upon comparison with our work, SliQ’s [23] impressive performance showcases the advantage of quantum computing in image processing. In the current methodology, we have adopted a scheme inspired by the work of SliQ, which utilizes the correlation between the computed model loss and the Euclidean distance to evaluate the performance of the model. This ingenious and transferrable approach addresses the challenge of objectively assessing image similarity in unlabeled datasets, proving effective within the limited application scenarios addressed in our work. However, this evaluation method remains open to refinement. For instance, explore more suitable correspondences between losses and classical image similarity detection methods within different numerical ranges. This refinement process stands as a significant future endeavor within our research trajectory.

During the construction process of A, P, N triplets, we employed noise to generate perturbed versions of reference images as positive instances within the triplets, and the efficacy of this strategy was validated through subse-

quent experimental analysis. While noise is conventionally perceived as an impediment in both classical and quantum contexts — noise cuts both ways — it can also serve as a valuable asset for specific tasks [51]. Although noise mitigation techniques have been extensively explored in quantum computing, acknowledging noise as a potentially beneficial factor paves the way for novel approaches and methodologies.

6. Conclusion

The QUSL method proposed in this work represents an advanced quantum approach tailored to address the challenges inherent in image similarity detection. A series of numerical simulations and quantum computer experiments reveal a substantial enhancement in similarity detection correlation compared to contemporary quantum methodologies, accompanied by significant reductions in quantum resource utilization. These empirical findings underscore the promising potential of the QUSL framework in effectively modeling similarity within expansive, unlabeled image datasets. Additionally, as a methodological framework, it exhibits transferability across diverse task scenarios. Further exploration of QUSL will revolve around more precise and objective similarity assessment and the utilization of noise for enhanced performance.

Authors’ contributions

Lian-Hui Yu: Methodology, Software. **Xiao-Yu Li:** Conceptualization, Project administration. **Geng Chen:** Writing - Original Draft, Visualization. **Qin-Sheng Zhu:** Validation. **Hui Li:** Formal analysis. **Guo-Wu Yang:** Supervision.

Availability of supporting data

All data generated or analysed during this study are available and included in this published article. Code for our work has been open-sourced.

Acknowledgements

This work was supported by National Key R&D Program of China (Grant No.2018FYA0306703), the Open Fund of Advanced Cryptography and Sys-

tem Security Key Laboratory of Sichuan Province (Grant No. SKLACSS-202105), Chengdu Innovation and Technology Project (No.2021-YF05-02413-GX and 2021-YF09-00114-GX), Sichuan Province key research and development project (No.2022YFG0315).

References

- [1] E. Knill, Quantum computing, *Nature* 463 (7280) (2010) 441–443. doi:<https://doi.org/10.1038/463441a>.
- [2] J. Preskill, Quantum computing in the nisq era and beyond, *Quantum* 2 (2018) 79. doi:<https://doi.org/10.22331/q-2018-08-06-79>.
- [3] F. Arute, K. Arya, R. Babbush, D. Bacon, J. C. Bardin, R. Barends, R. Biswas, S. Boixo, F. G. Brandao, D. A. Buell, et al., Quantum supremacy using a programmable superconducting processor, *Nature* 574 (7779) (2019) 505–510. doi:<https://doi.org/10.1038/s41586-019-1666-5>.
- [4] H.-Y. Huang, M. Broughton, J. Cotler, S. Chen, J. Li, M. Mohseni, H. Neven, R. Babbush, R. Kueng, J. Preskill, et al., Quantum advantage in learning from experiments, *Science* 376 (6598) (2022) 1182–1186. doi:<https://doi.org/10.1126/science.abn7293>.
- [5] H.-Y. Huang, M. Broughton, M. Mohseni, R. Babbush, S. Boixo, H. Neven, J. R. McClean, Power of data in quantum machine learning, *Nature communications* 12 (1) (2021) 2631. doi:<https://doi.org/10.1038/s41467-021-22539-9>.
- [6] X.-Y. Li, Q.-S. Zhu, Y. Hu, H. Wu, G.-W. Yang, L.-H. Yu, G. Chen, A new quantum machine learning algorithm: split hidden quantum markov model inspired by quantum conditional master equation, *Quantum* 8 (2024) 1232. doi:<https://doi.org/10.22331/q-2024-01-24-1232>.
- [7] J. Biamonte, P. Wittek, N. Pancotti, P. Rebentrost, N. Wiebe, S. Lloyd, Quantum machine learning, *Nature* 549 (7671) (2017) 195–202. doi:<https://doi.org/10.1038/nature23474>.
- [8] M. Schuld, I. Sinayskiy, F. Petruccione, The quest for a quantum neural network, *Quantum Information Processing* 13 (2014) 2567–2586. doi:<https://doi.org/10.1007/s11128-014-0809-8>.

- [9] M. Schuld, I. Sinayskiy, F. Petruccione, An introduction to quantum machine learning, *Contemporary Physics* 56 (2) (2015) 172–185. doi:<https://doi.org/10.1080/00107514.2014.964942>.
- [10] I. Cong, S. Choi, M. D. Lukin, Quantum convolutional neural networks, *Nature Physics* 15 (12) (2019) 1273–1278. doi:<https://doi.org/10.1038/s41567-019-0648-8>.
- [11] D. Silver, T. Patel, D. Tiwari, Quilt: Effective multi-class classification on quantum computers using an ensemble of diverse quantum classifiers, in: *Proceedings of the AAAI Conference on Artificial Intelligence*, Vol. 36, (2022), pp. 8324–8332. doi:<https://doi.org/10.1609/aaai.v36i8.20807>.
- [12] Y. Xu, X. Liu, X. Cao, C. Huang, E. Liu, S. Qian, X. Liu, Y. Wu, F. Dong, C.-W. Qiu, et al., Artificial intelligence: A powerful paradigm for scientific research, *The Innovation* 2 (4) (2021). doi:<https://doi.org/10.1016/j.xinn.2021.100179>.
- [13] X. Wang, Y. Du, S. Yang, J. Zhang, M. Wang, J. Zhang, W. Yang, J. Huang, X. Han, Retccl: Clustering-guided contrastive learning for whole-slide image retrieval, *Medical image analysis* 83 (2023) 102645. doi:<https://doi.org/10.1016/j.media.2022.102645>.
- [14] G. Cheng, J. Han, X. Lu, Remote sensing image scene classification: Benchmark and state of the art, *Proceedings of the IEEE* 105 (10) (2017) 1865–1883. doi:<https://doi.org/10.1109/JPROC.2017.2675998>.
- [15] L. Zhang, L. Zhang, X. Mou, D. Zhang, Fsim: A feature similarity index for image quality assessment, *IEEE transactions on Image Processing* 20 (8) (2011) 2378–2386. doi:<https://doi.org/10.1109/TIP.2011.2109730>.
- [16] G. Palubinskas, Image similarity/distance measures: what is really behind mse and ssim?, *International Journal of Image and Data Fusion* 8 (1) (2017) 32–53. doi:<https://doi.org/10.1080/19479832.2016.1273259>.
- [17] Y. Bai, H. Ding, S. Bian, T. Chen, Y. Sun, W. Wang, Simgnn: A neural network approach to fast graph similarity computation, in: *Proceedings of the twelfth ACM international conference on web search and data mining*, (2019), pp. 384–392. doi:<https://doi.org/10.1145/3289600.3290967>.
- [18] J. Wang, Y. Song, T. Leung, C. Rosenberg, J. Wang, J. Philbin, B. Chen, Y. Wu, Learning fine-grained image similarity with deep ranking, in: *Proceedings of the IEEE conference on computer vision and pattern recognition*,

- (2014), pp. 1386–1393.
 URL https://openaccess.thecvf.com/content_cvpr_2014/html/Wang_Learning_Fine-grained_Image_2014_CVPR_paper.html
- [19] Y. Dang, N. Jiang, H. Hu, Z. Ji, W. Zhang, Image classification based on quantum k-nearest-neighbor algorithm, *Quantum Information Processing* 17 (2018) 1–18. doi:<https://doi.org/10.1007/s11128-018-2004-9>.
 - [20] X. Liu, R.-G. Zhou, A. El-Rafei, F.-X. Li, R.-Q. Xu, Similarity assessment of quantum images, *Quantum Information Processing* 18 (2019) 1–19. doi:<https://doi.org/10.1007/s11128-019-2357-8>.
 - [21] R.-G. Zhou, Y.-J. Sun, Quantum multidimensional color images similarity comparison, *Quantum Information Processing* 14 (2015) 1605–1624. doi:<https://doi.org/10.1007/s11128-014-0849-0>.
 - [22] F. Yan, P. Q. Le, A. M. Ilyasu, B. Sun, J. A. Garcia, F. Dong, K. Hirota, Assessing the similarity of quantum images based on probability measurements, in: *2012 IEEE Congress on Evolutionary Computation*, IEEE, (2012), pp. 1–6. doi:<https://doi.org/10.1109/CEC.2012.6256418>.
 - [23] D. Silver, T. Patel, A. Ranjan, H. Gandhi, W. Cutler, D. Tiwari, Sliq: quantum image similarity networks on noisy quantum computers, in: *Proceedings of the AAAI Conference on Artificial Intelligence*, Vol. 37, (2023), pp. 9846–9854. doi:<https://doi.org/10.1609/aaai.v37i8.26175>.
 - [24] H. Wang, Y. Ding, J. Gu, Y. Lin, D. Z. Pan, F. T. Chong, S. Han, Quantumnas: Noise-adaptive search for robust quantum circuits, in: *2022 IEEE International Symposium on High-Performance Computer Architecture (HPCA)*, IEEE, 2022, pp. 692–708. doi:<https://doi.org/10.1109/HPCA53966.2022.00057>.
 - [25] N. Mohseni, P. L. McMahon, T. Byrnes, Ising machines as hardware solvers of combinatorial optimization problems, *Nature Reviews Physics* 4 (6) (2022) 363–379. doi:<https://doi.org/10.1038/s42254-022-00440-8>.
 - [26] M. Pirhooshayan, T. Terlaky, Quantum circuit design search, *Quantum Machine Intelligence* 3 (2021) 1–14. doi:<https://doi.org/10.1007/s42484-021-00051-z>.
 - [27] A. Zhang, S. Zhao, Evolutionary-based searching method for quantum circuit architecture, *Quantum Information Processing* 22 (7) (2023) 283. doi:<https://doi.org/10.1007/s11128-023-04033-x>.

- [28] L. Ding, L. Spector, Evolutionary quantum architecture search for parametrized quantum circuits, in: Proceedings of the Genetic and Evolutionary Computation Conference Companion, (2022), pp. 2190–2195. doi:<https://doi.org/10.1145/3520304.3534012>.
- [29] G. Krylov, M. Lukac, Quantum encoded quantum evolutionary algorithm for the design of quantum circuits, in: Proceedings of the 16th ACM International Conference on Computing Frontiers, (2019), pp. 220–225. doi:<https://doi.org/10.1145/3310273.3322826>.
- [30] R. Rasconi, A. Oddi, An innovative genetic algorithm for the quantum circuit compilation problem, in: Proceedings of the AAAI conference on artificial intelligence, Vol. 33, (2019), pp. 7707–7714. doi:<https://doi.org/10.1609/aaai.v33i01.33017707>.
- [31] J. Eisert, Entangling power and quantum circuit complexity, Physical Review Letters 127 (2) (2021) 020501. doi:<https://doi.org/10.1103/PhysRevLett.127.020501>.
- [32] M. Benedetti, E. Lloyd, S. Sack, M. Fiorentini, Parameterized quantum circuits as machine learning models, Quantum Science and Technology 4 (4) (2019) 043001. doi:<https://doi.org/10.1088/2058-9565/ab4eb5>.
- [33] A. Pérez-Salinas, A. Cervera-Liarta, E. Gil-Fuster, J. I. Latorre, Data re-uploading for a universal quantum classifier, Quantum 4 (2020) 226. doi:<https://doi.org/10.22331/q-2020-02-06-226>.
- [34] M. Cerezo, A. Arrasmith, R. Babbush, S. C. Benjamin, S. Endo, K. Fujii, J. R. McClean, K. Mitarai, X. Yuan, L. Cincio, et al., Variational quantum algorithms, Nature Reviews Physics 3 (9) (2021) 625–644. doi:<https://doi.org/10.1038/s42254-021-00348-9>.
- [35] L. Arufe, M. A. González, A. Oddi, R. Rasconi, R. Varela, Quantum circuit compilation by genetic algorithm for quantum approximate optimization algorithm applied to maxcut problem, Swarm and Evolutionary Computation 69 (2022) 101030. doi:<https://doi.org/10.1016/j.swevo.2022.101030>.
- [36] L. Arufe, R. Rasconi, A. Oddi, R. Varela, M. A. González, New coding scheme to compile circuits for quantum approximate optimization algorithm by genetic evolution, Applied Soft Computing 144 (2023) 110456. doi:<https://doi.org/10.1016/j.asoc.2023.110456>.

- [37] S. Altares-López, A. Ribeiro, J. J. García-Ripoll, Automatic design of quantum feature maps, *Quantum Science and Technology* 6 (4) (2021) 045015. doi:<https://doi.org/10.1088/2058-9565/ac1ab1>.
- [38] W. Wu, G. Yan, X. Lu, K. Pan, J. Yan, Quantumdarts: differentiable quantum architecture search for variational quantum algorithms, in: *International Conference on Machine Learning*, PMLR, (2023), pp. 37745–37764. URL <https://proceedings.mlr.press/v202/wu23v.html>
- [39] A. Veit, S. Belongie, T. Karaletsos, Conditional similarity networks, in: *Proceedings of the IEEE conference on computer vision and pattern recognition*, (2017), pp. 830–838. URL https://openaccess.thecvf.com/content_cvpr_2017/html/Veit_Conditional_Similarity_Networks_CVPR_2017_paper.html
- [40] K. He, H. Fan, Y. Wu, S. Xie, R. Girshick, Momentum contrast for unsupervised visual representation learning, in: *Proceedings of the IEEE/CVF conference on computer vision and pattern recognition*, (2020), pp. 9729–9738. URL https://openaccess.thecvf.com/content_CVPR_2020/html/He_Momentum_Contrast_for_Unsupervised_Visual_Representation_Learning_CVPR_2020_paper.html
- [41] D. Hendrycks, T. Dietterich, Benchmarking neural network robustness to common corruptions and perturbations, *arXiv preprint arXiv:1903.12261* (2019). URL <https://arxiv.org/abs/1903.12261>
- [42] P. Rebentrost, M. Mohseni, S. Lloyd, Quantum support vector machine for big data classification, *Physical review letters* 113 (13) (2014) 130503. doi:<https://doi.org/10.1103/PhysRevLett.113.130503>.
- [43] A. E. Paine, V. E. Elfving, O. Kyriienko, Quantum kernel methods for solving regression problems and differential equations, *Physical Review A* 107 (3) (2023) 032428. doi:<https://doi.org/10.1103/PhysRevA.107.032428>.
- [44] Y. Nam, N. J. Ross, Y. Su, A. M. Childs, D. Maslov, Automated optimization of large quantum circuits with continuous parameters, *npj Quantum Information* 4 (1) (2018) 23. doi:<https://doi.org/10.1038/s41534-018-0072-4>.
- [45] H. Fang, Q. Wang, Y.-C. Tu, M. F. Horstemeyer, An efficient non-dominated sorting method for evolutionary algorithms, *Evolutionary computation* 16 (3) (2008) 355–384. doi:<https://doi.org/10.1162/evco.2008.16.3.355>.

- [46] Y. Mei, Y. Fan, Y. Zhang, J. Yu, Y. Zhou, D. Liu, Y. Fu, T. S. Huang, H. Shi, Pyramid attention network for image restoration, *International Journal of Computer Vision* 131 (12) (2023) 3207–3225. doi:<https://doi.org/10.1007/s11263-023-01843-5>.
- [47] Y. Men, Y. Yao, M. Cui, Z. Lian, X. Xie, X.-S. Hua, Unpaired cartoon image synthesis via gated cycle mapping, in: *Proceedings of the IEEE/CVF conference on computer vision and pattern recognition*, (2022), pp. 3501–3510.
URL https://openaccess.thecvf.com/content/CVPR2022/html/Men_Unpaired_Cartoon_Image_Synthesis_via_Gated_Cycle_Mapping_CVPR_2022_paper.html
- [48] T.-Y. Lin, M. Maire, S. Belongie, J. Hays, P. Perona, D. Ramanan, P. Dollár, C. L. Zitnick, Microsoft coco: Common objects in context, in: *Computer Vision–ECCV 2014: 13th European Conference, Zurich, Switzerland, September 6–12, 2014, Proceedings, Part V 13*, Springer, (2014), pp. 740–755. doi:https://doi.org/10.1007/978-3-319-10602-1_48.
- [49] M. Douze, G. Tolias, E. Pizzi, Z. Papakipos, L. Chanussot, F. Radenovic, T. Jenicek, M. Maximov, L. Leal-Taixé, I. Elezi, et al., The 2021 image similarity dataset and challenge, *arXiv preprint arXiv:2106.09672* (2021).
URL <https://arxiv.org/abs/2106.09672>
- [50] M. Developer, Mindquantum, version 0.9.11 (March 2021).
URL <https://gitee.com/mindspore/mindquantum>
- [51] D. Liu, W. Li, L. Duan, I. W. Tsang, G. Yang, Noisy label learning with provable consistency for a wider family of losses, *IEEE Transactions on Pattern Analysis and Machine Intelligence* (2023). doi:<https://doi.org/10.1109/TPAMI.2023.3296156>.

Appendix A. The quantum circuits obtained by QUSL

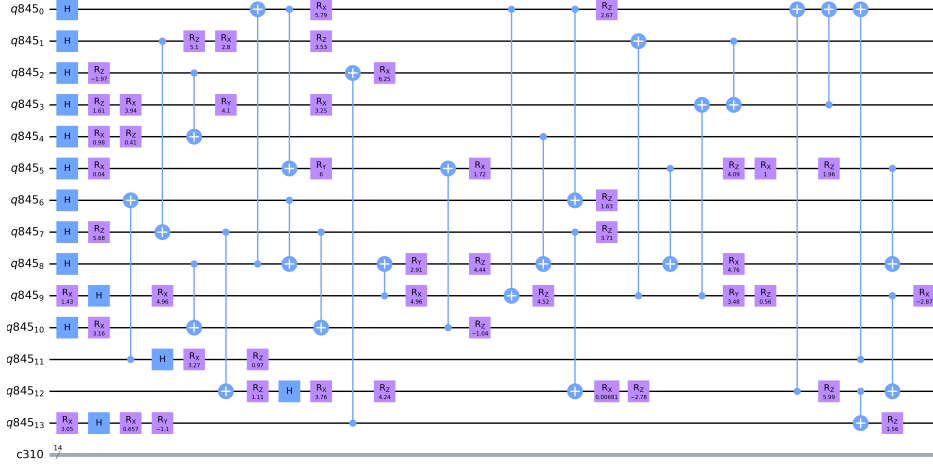


Figure A.10: The optimal-performing quantum circuit obtained by QUSL on the landscape dataset exhibits a correlation performance of 0.889, with 26 CNOT operations and a circuit depth of 28.

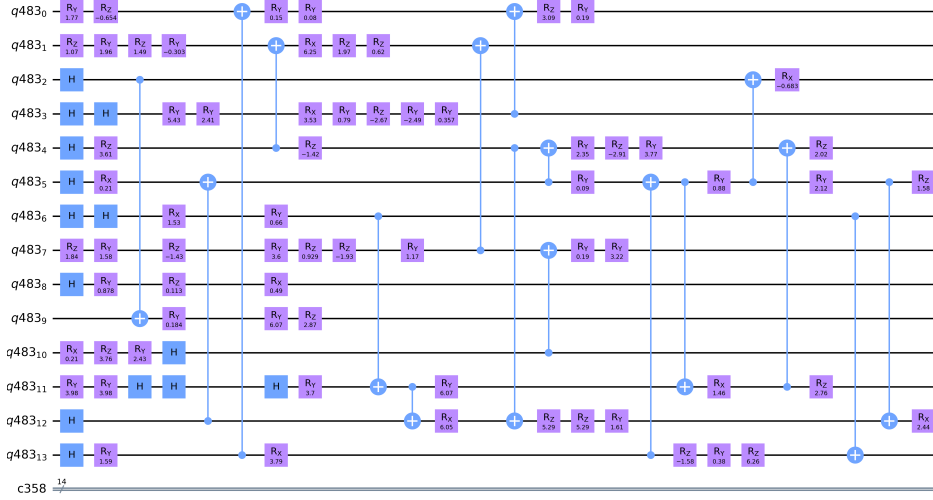


Figure A.11: The optimal-performing quantum circuit obtained by QUSL on the DISC21 dataset exhibits a correlation performance of 0.861, with 17 CNOT operations and a circuit depth of 26.

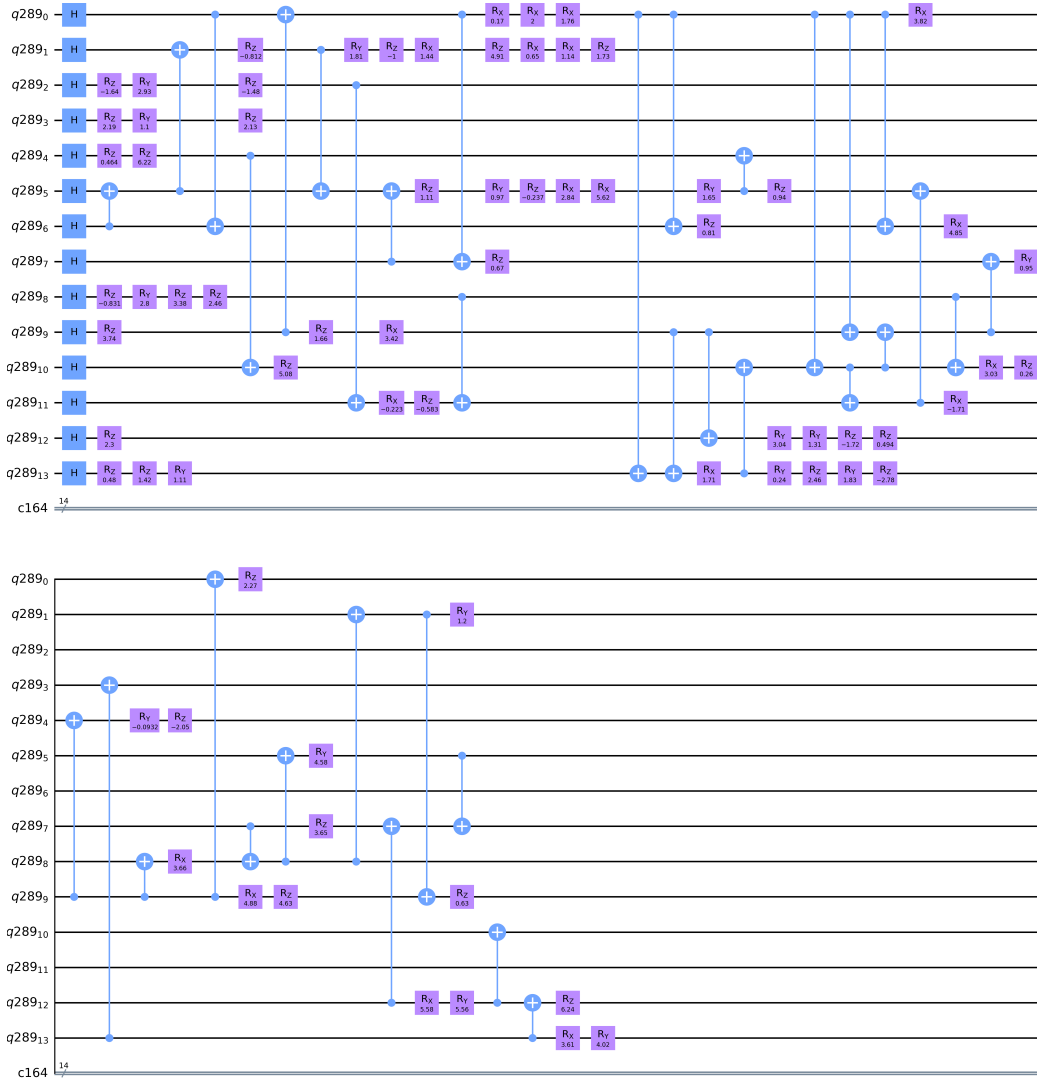


Figure A.12: The optimal-performing quantum circuit obtained by QUSL on the COCO dataset exhibits a correlation performance of 0.876, with 36 CNOT operations and a circuit depth of 44.

Appendix B. Quantum circuits with similar fitness but significantly different structures



Figure B.13: Quantum circuits with significant structural differences but similar fitness levels during training. These circuits are derived from the training process on the COCO dataset, exhibiting fitness differences on the order of 10^{-4} , yet their quantum circuit depths and CNOT counts differ by almost a factor of two.

Appendix C. The model’s performance in classification tasks

We extend our evaluation to include multi-classification tasks as simplified instances of image similarity tasks as explained in the introduction, offering insights into QUSL’s performance. Rigorous binary classification experiments on three widely recognized multi-classification datasets — mnist, fashion-mnist, and AIDS — aim to validate the model’s usability and assess its performance under simplified scenarios. Table Appendix C compares the performance of SliQ and QUSL on three multi-classification datasets.

Table C.6: The comparison between QUSL and SliQ in terms of classification task accuracy

Dataset	SliQ	QUSL (ours)
mnist	97.16(± 0.193)	98.50(± 0.235)
fashion-mnist	92.53(± 0.409)	92.76(± 0.682)
AIDS	71.54(± 0.257)	71.32(± 0.457)

In classification tasks, QUSL and SliQ exhibit similar accuracy, but with slightly reduced robustness in the case of QUSL. This may be attributed to the heuristic algorithm-based quantum circuit design facing more pronounced challenges related to population diversity in simpler image classification tasks, thereby inducing instability in the model.